PNAS
www.pnas.org

Supplementary Information for

Multidimensional four-wave mixing signals detected by quantum squeezed-light

Konstantin Dorfman[a,1,2], Shengshuai Liu[a,1], Yanbo Lou[a,1], Tianxiang Wei[a], Jietai Jing[a,b,c,d,2], Frank Schlawin[e], and Shaul Mukamel[f]

[2] **Konstantin Dorfman E-mail: dorfmank@lps.ecnu.edu.cn;**
[2]**Jietai Jing E-mail: jtjing@phy.ecnu.edu.cn**

This PDF file includes:

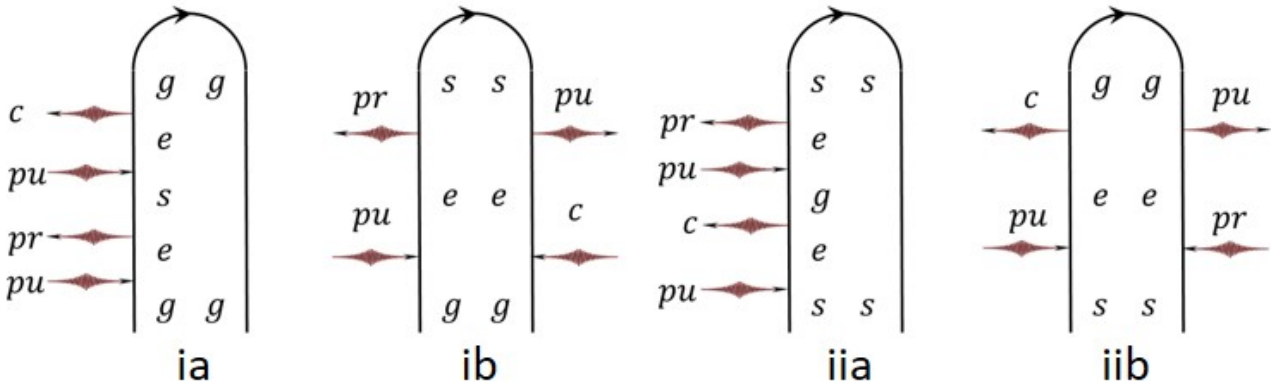

Fig. S1. Diagrams representing the third order susceptibility for the level scheme in Fig. 1b.

Supporting Information Text

S1. Perturbative treatment of weak fields

The field/matter interaction Hamiltonian is

$$H_{FWM} = \int d\mathbf{r}\mu_{eg}(E_c(t,\mathbf{r}) + E_{pu}(t,\mathbf{r})) + \mu_{es}E_{pr}(t,\mathbf{r}), \quad [S1]$$

where the classical pump field $E_{pu}(t,\mathbf{r}) = \mathcal{E}_{pu}e^{-i\omega_{pu}t+i\mathbf{k}_{pu}\cdot\mathbf{r}}$ and the probe and conjugate are quantum fields given by

$$E_j(t,\mathbf{r}) = \sqrt{\frac{2\pi\hbar\omega_j}{V}}(\hat{a}_j e^{-i\omega_j t+i\mathbf{k}_j\cdot\mathbf{r}} + \hat{a}_j^\dagger e^{i\omega_j t-i\mathbf{k}_j\cdot\mathbf{r}}), \quad j = pr, c \quad [S2]$$

We use classical fields to calculate susceptibility components in Eqs. (S11)- (S12), while the quantum nature of the fields is utilized for input-output relations in Eqs. (S13) - (S14) which lead to Eqs. (1) – (2) of the main text. The applicability of classical fields to calculate susceptibility components is a standard procedure. Some discrepancies in susceptibilities at single photon level may be observed, which is not the case for many-photon squeezed light. Lowering and raising operators commonly used with dipole interaction Hamiltonian and two- and three-level quantum system also apply in this case. We thus replace the operators of the probe and conjugate fields by their respective expectation values: $\mathcal{E}_{pr} = \sqrt{\frac{2\pi\hbar\omega_{pr}}{V}}\langle\hat{a}_{pr}\rangle$ and $\mathcal{E}_c = \sqrt{\frac{2\pi\hbar\omega_c}{V}}\langle\hat{a}_c\rangle$. The third-order perturbative approach is visualized by the loop diagrams shown in Fig. S1. In diagrams *ia* and *ib* the initial state is the ground state g, whereas in diagrams *iia* and *iib* s is the initial state. At high temperatures both g and s state are almost equally populated. The Schrodinger equation for the state amplitudes

$$|\psi(t)\rangle = [c_g(t)|g\rangle + c_s(t)|s\rangle]e^{i(\omega_{pu}-\omega_e)t} + c_e(t)e^{-i\omega_e t}|e\rangle \quad [S3]$$

is given by

$$\begin{aligned}
\dot{c}_g &= -i\delta_{eg}c_g - i\Omega_{eg}^* c_e - i\Omega_c^* e^{i(\omega_c-\omega_{pu})t}c_e,\\
\dot{c}_s &= -i\delta_{es}c_s - i\Omega_{es}^* c_e - i\Omega_{pr}^* e^{i(\omega_{pr}-\omega_{pu})t}c_e,\\
\dot{c}_e &= -i\Omega_{eg}c_g - i\Omega_{es}c_s - i\Omega_c e^{-i(\omega_c-\omega_{pu})t}c_g - i\Omega_{pr}e^{-i(\omega_{pr}-\omega_{pu})t}c_s,
\end{aligned} \quad [S4]$$

where $\delta_{em} = \omega_{pu} - \omega_{em}$, $m = g, s$, $\Omega_c = \mu_{eg}\mathcal{E}_c$, $\Omega_{pr} = \mu_{es}\mathcal{E}_{pr}$, and for brevity we omitted the subscript of the e state in detunings δ_{em} and Rabi frequencies Ω_{e_m} treating e_1 and e_2 in a similar fashion. Initial conditions fo Eq. (S4) are $c_g(t_0) = 1$, $c_e(t_0) = c_s(t_0) = 0$ for ia, ib diagrams and $c_s(t_0) = 1$, $c_g(t_0) = c_e(t_0) = 0$ for iia, iib diagrams. Instead of simply reading the signal form the diagrams in Fig. S1 we deliberately indicate some important steps which will be further used in the strong pump case. We focus on diagram ia. Other diagrams can be treated similarly. To derive third order susceptibility we define a signal first, which according to the diagram ia is given as a transmission of the conjugate beam:

$$S_{ia}(t) = \mathrm{Im}[\mathcal{E}_c^*(t)P_{ia}^{(3)}(t)], \quad [S5]$$

where third order polarization is given by

$$P_{ia}^{(3)}(t) = \mu_{eg}c_e^{(3)}(t)c_g^{(0)*}(t). \quad [S6]$$

Konstantin Dorfman[a,1,2], Shengshuai Liu[a,1], Yanbo Lou[a,1], Tianxiang Wei[a], Jietai Jing[a,b,c,d,2], Frank Schlawin[e], and Shaul Mukamel[f]

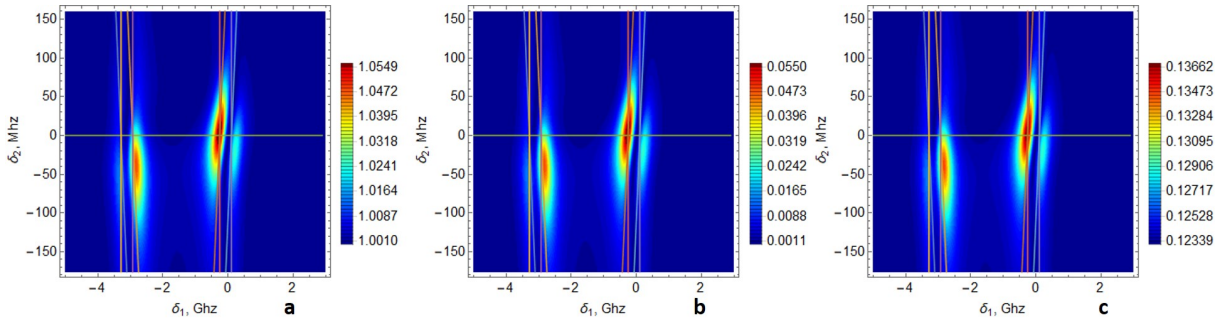

Fig. S2. Calculated perturbative 2D spectra of the probe Eq. (1) with gain governed by perturbative susceptibilities given by Eqs. (S11) - (S12) displayed vs one - δ_1 and two-photon δ_2 detunings - (a), conjugate - (b) and squeezing - (c).

For the weak pump field perturbative orders are taken for all three fields: pump, probe and conjugate. Zeroth order term $c_g^{(0)}(t) = e^{-i\delta_{eg}(t-t_0)}$. Third order amplitude $c_e^{(3)}$ can be calculated in a sequence of 3 steps according to field-matter interactions in diagram ia:

$$c_e^{(3)}(t) = -i\delta_{es}\int_{t_0}^{t} dt' c_s^{(2)}(t'), \tag{S7}$$

where

$$c_s^{(2)}(t') = -i\Omega_{pr}^{*}\int_{t_0}^{t'} dt'' e^{i(\omega_{pr}-\omega_{pu})t''} c_e^{(1)}(t''), \tag{S8}$$

where

$$c_e^{(1)}(t'') = -i\Omega_{eg}\int_{t_0}^{t''} dt''' c_g^{(0)}(t'''). \tag{S9}$$

Solving Eqs. (S7) - (S9) and taking the limit $t_0 \to -\infty$ we obtain

$$P_{ia}^{(3)}(t) = \chi_{ia}^{(3)}(-\omega_{pr}, -\omega_c; 2\omega_{pu})\mathcal{E}_{pu}^2\mathcal{E}_{pr}^{*}e^{-i(2\omega_{pu}-\omega_{pr})t} \tag{S10}$$

where

$$\chi_{ia}^{(3)}(-\omega_{pr}, -\omega_c; 2\omega_{pu}) = \sum_e \frac{|\mu_{eg}|^2|\mu_{es}|^2}{(2\omega_{pu}-\omega_{pr}-\omega_{eg}+i\gamma_e)(\omega_{pu}-\omega_{pr}-\omega_s+i\gamma_{sg})(\omega_{pu}-\omega_{eg}+i\gamma_e)}. \tag{S11}$$

Similarly we obtain for other diagrams:

$$\begin{aligned}
\chi_{ib}^{(3)}(-\omega_{pr}, -\omega_c; 2\omega_{pu}) &= \sum_e \frac{|\mu_{eg}|^2|\mu_{es}|^2}{(\omega_c-\omega_{eg}-i\gamma_e)(\omega_c-\omega_{pu}-\omega_{sg}-i\gamma_s)(\omega_{pu}-\omega_{eg}+i\gamma_e)}, \\
\chi_{iia}^{(3)}(-\omega_{pr}, -\omega_c; 2\omega_{pu}) &= \sum_e \frac{|\mu_{eg}|^2|\mu_{es}|^2}{(2\omega_{pu}-\omega_c-\omega_{es}+i\gamma_e)(\omega_{pu}-\omega_c-\omega_{gs}+i\gamma_s)(\omega_{pu}-\omega_{es}+i\gamma_e)}, \\
\chi_{iib}^{(3)}(-\omega_{pr}, -\omega_c; 2\omega_{pu}) &= \sum_e \frac{|\mu_{eg}|^2|\mu_{es}|^2}{(\omega_{pr}-\omega_{es}-i\gamma_e)(\omega_{pr}-\omega_{pu}-\omega_{gs}-i\gamma_s)(\omega_{pu}-\omega_{es}+i\gamma_e)},
\end{aligned} \tag{S12}$$

where dephasing rates have been added phenomonologically. The total susceptibility thus is given by $\chi^{(3)} = \sum_k A_k\tilde{\chi}_k^{(3)}$, where A_k are normalization functions that depend on the propagation length inside the sample and other experimental parameters, k runs over the diagrams $k = ia, ib, iia, iib$. Note, that we included normalization constant into the susceptibility itself, for brevity. The quantum state of light generated via FWM is given by $|\psi_{FWM}\rangle = U|\psi\rangle_0$ where $|\psi\rangle_0$ is the incoming state of light before the FWM. The unitary evolution operator $U = \exp\left(\chi^{(3)}\hat{a}_{pr}^{\dagger}\hat{a}_c^{\dagger}/2 - h.c.\right)$, where we utilized the quantum nature of the probe and conjugate fields by bringinig back their original operator form.

The corresponding input-output relation is given by

$$\hat{a}_{pr} = U^{\dagger}\hat{a}_{pr0}U = \cosh(s)\hat{a}_{pr0} + e^{i\theta}\sinh(s)\hat{a}_{c0}^{\dagger}, \tag{S13}$$

$$\hat{a}_c^{\dagger} = U^{\dagger}\hat{a}_{c0}^{\dagger}U = e^{-i\theta}\sinh(s)\hat{a}_{pr0} + \cosh(s)\hat{a}_{c0}^{\dagger}, \tag{S14}$$

where $s = |\chi^{(3)}|$. The corresponding photon number of the probe, conjugate, and noise figure are given by Eqs. (1) - (2) of the main text and depicted in Fig. S2a, b, and c, respectively. The 2D spectrograms indicate four peaks equivalent to $\delta_1 = 0$, $\delta_1 = -\omega_s$, and $\delta_2 = 0$. There are no Stark shifts associated with the strong field observed in experiment. We notice, that the probe gain is of the order of 1 which results in the absence of amplification and low (10^{-2}) level of the conjugate gain. The corresponding squeezing is also small and positive (classical). It is therefore clear, that stronger pump is required to observe high gain and low noise figure.

S2. Strong pump

When the pump is strong, perturbation theory can be only applied to the probe and conjugate fields. In this case, nonlinear polarization is given by

$$P_{ia}^{(3)}(t) = \mu_{eg} c_e^{(1)}(t) c_g^{(0)*}(t), \tag{S15}$$

where zeroth order amplitude $c_g^{(0)}$ satisfy the following system of equations:

$$\begin{aligned} \dot{c}_g^{(0)} &= -i\delta_{eg} c_g^{(0)} - i\Omega_{eg}^* c_e^{(0)}, \\ \dot{c}_e^{(0)} &= -i\Omega_{eg} c_g^{(0)} \end{aligned} \tag{S16}$$

Here we make one important ansatz. Since the AC Stark shift due to the strong pulse affects mostly two peaks 2 and 3 (see Fig. 2), we treat pump-driven transitions $g - e$ and $s - e$ separately. This allows to consider closed two sets of equations involving a pair of amplitudes only. As our results indicate, this ansatz allows to obtain reasonable agreement between peak positions. In this case, solution of Eq. (S16) reads

$$c_g^{(0)}(t) = e^{-\frac{1}{2}\delta_{eg}(t-t_0)} \left[\cos \Omega'_{eg}(t-t_0) - i \frac{\delta_{eg}}{2\Omega'_{eg}} \sin \Omega'_{eg}(t-t_0) \right], \tag{S17}$$

where $\Omega'_{eg} = \sqrt{\delta_{eg}^2/4 + \Omega_{eg}^2}$ and we assume real Rabi frequency $\Omega_{eg}^* = \Omega_{eg}$. Note, that the standard Rabi oscillations given by Eq. (S17) occur with both Stark shifted energies $\omega_{eg}^{(\pm)} = \delta_{eg}/2 \pm \Omega'_{eg}$. The corresponding $c_e^{(0)}$ amplitude is given by

$$c_e^{(0)} = \frac{\Omega_{eg}}{2\Omega'_{eg}} \left(e^{-i\omega_{eg}^{(+)}(t-t_0)} - e^{-i\omega_{eg}^{(-)}(t-t_0)} \right). \tag{S18}$$

The solution for the first order amplitude $c_e^{(1)}$ satisfies the following

$$\begin{aligned} \dot{c}_s^{(1)} &= -i\delta_{es} c_s^{(1)} - i\Omega_{es}^* c_e^{(1)} - i\Omega_{pr}^* e^{i(\omega_{pr}-\omega_{pu})t} c_e^{(0)}, \\ \dot{c}_e^{(1)} &= -i\Omega_{es} c_s^{(1)}. \end{aligned} \tag{S19}$$

Eq. (S19) can be solved exactly analytically. After a bit of algebra one can collect all the necessary terms and obtain an expression for the susceptibility ia and similarly for ib given by Eq. (3).

S3. Optical losses

Similar to the weak pump case, one can account for the optical losses associated with the elastic scattering of the pump into the photon with probe and conjugate frequencies. We define the optical loss coefficient in terms of the linear susceptibility:

$$\eta_r = \cos(|\tilde{\chi}_r^{(1)}|)^2, r = pr, c, \tag{S20}$$

where $\tilde{\chi}_r^{(1)}$ originate from the linear polarization:

$$P_c^{(1)}(t) = \mu_{eg} c_e^{(0)}(t) c_g^{0*}(t) \tag{S21}$$

Using Eq. (S17) and Eq. (S18) one obtains expression for $\tilde{\chi}_c^{(1)}(-\omega_c; \omega_{pu})$ given by Eq. (5). Similarly one can obtain $\tilde{\chi}_{pr}^{(1)}(-\omega_{pr}; \omega_{pu})$. The importance of the optical losses in experiment can be visualized if one would take a straightforward approach and plot the noise spectra in the absence of the optical losses in Eq. (2) using the data of Fig. 2d. The result shown in Fig. S3 indicates that there is no new information about the system. Rather noise spectra shown in Fig. S3 repeats Fig. 2d with a slightly different scaling. In contrast, real experimental data of the noise figure in Fig. 2f indicates new information accessible only in the presence of the optical losses.

S4. Coefficient of determination

We have calculated the coefficient of determination (R^2) defined as

$$R^2 = 1 - \frac{\sum_i (y_i - f_i)^2}{\sum_i (y_i - \bar{y})^2}, \tag{S22}$$

where y_i is the experimental value (black dots in Fig. 3), i=1,...,N. N is the number of the experimental values. $\bar{y}$ is the mean value of experimental values. f_i is the corresponding theory value of y_i (red line in Fig. 3). Based on Eq. (S22), the values of the coefficient of determination (R^2) in Fig. 3b, c, d, f, g, h are 0.41, 0.92, 0.72, 0.85, 0.58, 0.51, respectively. We added the corresponding values in the caption of Fig. 3.

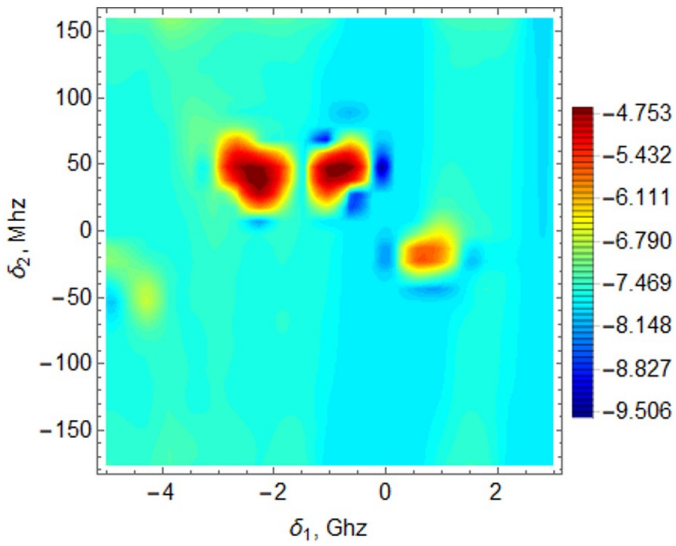

Fig. S3. Noise figure Eq. (2) in the absence of the optical losses for the gain G taken from Fig. 2d.

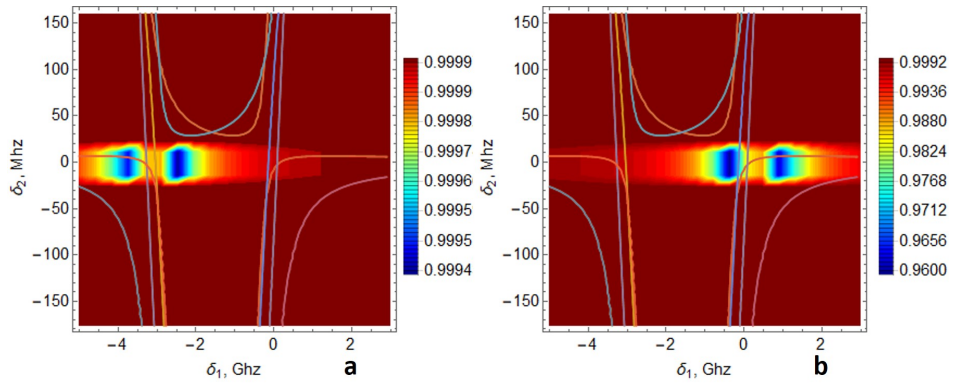

Fig. S4. 2D Spectra Eq. (S20) of the optical losses for the probe η_{pr} and conjugate η_c beams with susceptibilities given by Eq. (5).